IPPI

Polyolefins Journal, Vol. 1 No. 2 (2014) 77-91

ORIGINAL PAPER

# Modelling the catalyst fragmentation pattern in relation to molecular properties and particle overheating in olefin polymerization

Mohsen Najafi, Mahmoud Parvazinia*, Mir Hamid Reza Ghoreishy

Iran Polymer and Petrochemical Institute, P.O. Box: 14975/112, Tehran, Iran

Received: 14 November 2013, Accepted: 11 March 2014

## ABSTRACT

A two-dimensional single particle finite element model was used to examine the effects of particle fragmental pattern on the average molecular weights, polymerization rate and particle overheating in heterogeneous Ziegler-Natta olefin polymerization. A two-site catalyst kinetic mechanism was employed together with a dynamic two-dimensional molecular species in diffusion-reaction equation. The initial catalyst active sites distribution was assumed to be uniform, while the monomer diffusion coefficient was considered to be different inside the fragments and cracks. In other words, the cracks were distinguished from fragments with higher monomer diffusion coefficient. To model the particle temperature a lumped heat transfer model was used. The fragmentation pattern was considered to remain unchanged during the polymerization. A Galerkin finite element method was used to solve the resulting two-dimensional (2-D) moving boundary value, diffusion-reaction problem. A two-dimensional polymeric flow model (PFM) was implemented on the finite element meshes. The simulation results showed that the fragmentation pattern had effects on the molecular properties, reaction rate and the particle temperature at early stages of polymerization. **Polyolefins J (2014) 1:77-91**

**Keywords:** particle overheating; finite element method; modelling; particle growth; polyolefin

## INTRODUCTION

Polyolefins are commonly produced by low-pressure catalytic (e.g., Ziegler–Natta (Z–N), metallocenes, etc.) processes. The catalyst particles with size range of about 20 to 100 μm were continuously fed into the reactor to form polymer particles with size range of 50 to 5000 μm. Ziegler-Natta catalysts typically consist of $TiCl_3$ and TEA ($AlEt_3$) which are supported on porous $MgCl_2$ or silica particles. Polymerization proceeds at the active catalyst of Ti-sites distributed throughout the porous support. The polymer formed inside the porous catalyst, at the very early stages of polymerization, results in catalyst fragmentation.

A number of publications have appeared in open access literature on the mathematical modeling of catalyst/polymer particle growth in heterogeneous catalytic olefin polymerization [1-2]. The polymeric flow model (PFM) [3-9] and the multi-grain model (MGM) [10-15] are predominantly used generally with reasonable

* Corresponding Author - E-mail: M.Parvazinia@ippi.ac.ir

approximations. Moreover, these two models are also the basis for more complicated models in single particle modeling which are presented later in this article.

In multi-grain model, the particle consists of incorporated micro-particles and the reaction takes place at the surface of these micro-particles. The diffusion coefficients are different for macro- and micro-particle. The PFM offers the advantage of a relatively simpler mathematical formulation via the hypothesis of a pseudo-homogeneous reaction medium that greatly facilitates the numerical solution of the resulting moving boundary problem.

The PFM, first proposed by Schmeal et al. [3] and Singh et al. [4], describes the growing catalyst/polymer particle with a diffusion-reaction equation inside the particle. The particle growth is calculated based on the produced polymer by calculating the radius of the spherical particle in a one-dimensional model which is commonly used. Galvan et al. [5] used a mathematical transformation to convert the resulting moving-boundary value into a fixed-boundary condition. For highly active catalysts (e.g., polymerization rates over 30000 $g/g_{cat}.h$), internal and external mass and heat transfer phenomena can become extremely important and, thus, they need to be carefully accounted for in the development of a single particle model (SPM) [15-17]. Mc Kenna et al. [18] reviewed the strength and weakness of existing single particle models and demonstrated that they need improvements in the area of mass transfer models in the form of mechanistic description of particle morphology. In a publication by Veera et al. [8], they included monomer transport by convection to justify the high rate of polymerization and heat transfer. It was shown that monomer convection through particles' pores did add substantial contribution towards total monomer transport to catalyst active sites. There is no change reported on the effective monomer diffusion coefficient during polymerization due to particle evolving morphology in their work. Kosek et al. [19] employed two different diffusion models, namely, the dusty gas model and a Fickian diffusion model, to show the effect of convective flow of molecular species on particle temperature. Kanellopoulos et al. [9] developed a comprehensive single particle growth model and studied a number of parameters in a growing polymer particle. They investigated the effects of initial catalyst size, catalyst active sites concentration, catalyst/particle morphology, degree of polymer crystallinity, monomer sorption kinetics, catalyst pre-polymerization conditions and hydrodynamic flow conditions on the particle growth and particle overheating for highly active Ziegler-Natta catalysts in gas-phase olefin polymerization. Dompazis et al. [20] developed a multi-dynamic model for the determination of the distributed properties (i.e., PSD and MWD) and the extent of particle segregation in a catalytic gas-phase olefin copolymerization.

Catalyst/polymer particle fragmentation and breakage, particle growth and morphological development, particles agglomeration and fine particles formation and particle overheating are other challenging problems arise when heterogeneous catalysts are used for olefin polymerization [1-2]. These challenging problems have been the subject of a number of research attempts, for instance:

Ferrero et al. [21,22] developed a mathematical model to analyze and predict the fragmentation of support/catalyst particles during propylene polymerization. They considered the rupture phenomenon and showed an influence of catalyst structure on critical phenomena during early polymerization stages. Alexiadis et al. [23] in line with the model proposed by Ferrero et al. [21,22] and later by Bonini et al. [24] presented a new model based on MGM with a more sophisticated approach to fragmentation. Additionally, there is a more specific modeling for the unfragmented core.

Kittelson et al. [25] introduced a mathematical model describing the build-up and relaxation of elastic tensions inside growing particles during the heterogeneous polymerization of olefins, as mass transfer resistance would lead to spatial variation in the expansion rate of polymer which could create tension and lead to particle break up. Kittelson et al. [26] developed and demonstrated a new viscoelastic model to describe the fragmentation process of catalyst particles in olefin polymerization. In this model an idealized, equal-sized cylindrical and triangular pores were considered. The polymer production inside these pores was accompanied by formation of stress in the polymer, leading to small physical or chemical imperfections in the support material. Kittelson et al. [27] presented a three-level mass-transfer model for the heterogeneous polymerization of olefins. In comparison with traditional models (MGM) that included mass-transfer effects only at the macro- and micro-scales, these researchers considered the mass-transfer resistance at the meso level in explaining

particle morphology.

Grofet al. [28] developed a SPM to predict the morphogenesis of polyolefin particles at the early stages of polymerization. The simulation results of their model showed different morphological features such as fine particle formation, cracks formation inside polymer particles, hollow particles, good or poor replications of the shape of original catalyst particle, and the evolution of porous polymer particles could be achieved due to selected parameters in the model. Grof et al. [29] employed their developed model to study the morphogenesis of polyolefin particles by focusing on the effect of temperature and identify the reaction conditions leading to the disintegration of the growing particles into finer particles, which is the unwanted phenomenon observed in industrial reactors. Horackova et al. [30] demonstrated the capabilities of the advanced model and presented simple mappings between the architecture of catalyst carrier, reactor conditions and fragmentation patterns. They employed a morphogenesis model to address some selected experimental observations of the fragmentation stage of particle growth. Specifically, the capabilities of the model were demonstrated on the "shrinking core" and the "continuous bisection" fragmentation mode of porous catalyst carriers. Since the dynamics of sorption/desorption of reactants/diluents in porous polyolefin particles are one of the important phenomena both during polymerization and in post-processing of polymer powder. Bobak et al. [31] proposed a particle model including two sizes of compact polymer granules and demonstrated that the degassing of the powder in the down-stream processing could be described by this model and that the model was capable of estimating the fractions of large and small compact zones and the size of large compact zones by just studying the fragmentation pattern.

Machado et al. [32] analyzed the very early development of particle morphology and polymer properties for three different commercial catalyst systems: $MgCl_2$ - and $SiO_2$-supported Ziegler–Natta and $SiO_2$-supported metallocene. It was shown that, depending on the operating conditions, distinct non-uniform catalyst fragmentation patterns may develop; confirming different scenarios described by published fragmentation models. In addition, it was shown that the molecular weight distributions and polymer yields, obtained during the very early stages of the polymerization, suggested the existence of significant temperature gradients inside the growing polymer particles.

In all the above research reports, in spite of the development of complicated models using a one-dimensional model the effect of fragmentation and morphology complexities was not studied on the molecular properties of the final polymer properly. Although many attempts have been made to model the transport phenomenon at different scales namely macro, meso and micro-scale to account for morphological complexities but only radial variations can be included in a one-dimensional model.

Najafi et al. [33] proposed an isothermal 2-D computational model based on PFM assumption to include geometrical and structural complexities in the model. They showed that initial particle shape and particle breakage have considerable effects on reaction rate and molecular properties of the resulting polymer.

In their study, using the developed 2-D model Najafi et al. [33] estimated the effect of cracks inside the particle by fragmentation on the molecular properties of the polymer and particle overheating. In solving diffusion-reaction equation inside the particle, the cracks and fragments were distinguished by different monomer diffusion coefficients. The monomer diffusion coefficient inside the cracks was considered to be higher than inside the fragments but these different coefficients remained unchanged in the course of polymerization reaction. Since a growing particle was modeled the moving boundary of the computational domain was identified by a fill factor at each timing step. The lumped energy equation was used to calculate the particle temperature in the course of polymerization reaction.

Simulation results show that the fragmentation patterns affect the molecular properties and reaction rate. It is also shown that fragmentation patterns have significant effect on the particle temperature at the early stages of polymerization. The results show that in the case of radial cracks inside the particle, a low film heat transfer coefficient inside the cracks has a significant role in enhancing heat transfer to reduce overheating. In the present work it is assumed that no crack propagation occurs in the course of polymerization reaction. In other words the number of cracks remains unchanged.

## Model development

*Kinetic mechanism and polymerization rate functions*

To calculate the monomer consumption rate and

polymer molecular weight developments in a heterogeneous multi-site Z-N catalyst, a two-active site catalytic mechanism is employed. The kinetic mechanism is comprised of a series of elementary reactions, including site activation, chain initiation, propagation, transfer $P_n^k$ and $D_n^k$ catalyst deactivation (Table1). The symbols $P_n^k$ and $D_n^k$ denote the concentrations of 'live' and 'dead' polymer chains of total length n, formed at the 'k' catalyst active site respectively. The symbols $C^k$, $C^{*k}$ and $C_d^k$ denote the concentrations of fresh, activated and deactivated catalyst sites of type 'k'. Based on the assumed kinetic mechanism (Table 1), the following 'live' $\lambda_\nu^k$ and 'dead' $\mu_\nu^k$ moments of the corresponding number chain length distributions [33-35] can be defined as:

$$\lambda_\nu^k = \sum_{n=1}^{\infty} n^\nu P_n^k \quad , \quad \mu_\nu^k = \sum_{n=2}^{\infty} n^\nu D_n^k \qquad (1)$$

Accordingly, the total monomer consumption rate can be written as

$$R_P = -\frac{d[M]}{dt} = \sum_{k=1}^{2} \left( K_P^k \left[\lambda_0^k\right] + K_i^k \left[C^{*k}\right] \right)[M] \qquad (2)$$

The net production/consumption rates of all other molecular species are reported in Table 2. The numerical values of all the kinetic rate constants, employed in the present study, are given in Table 3 (based on values presented by Floyd et al. [11-13]). To calculate the number and weight average chain lengths of the polymer chains produced over the two-site catalyst ($\overline{X}_n$ and $\overline{X}_w$), the following equations are employed:

$$\overline{X}_n = \frac{\sum_{k=1}^{2} \lambda_1^k + \mu_1^k}{\sum_{k=1}^{2} \lambda_0^k + \mu_0^k} \quad ; \quad \overline{X}_w = \frac{\sum_{k=1}^{2} \lambda_2^k + \mu_2^k}{\sum_{k=1}^{2} \lambda_1^k + \mu_1^k} \qquad (3)$$

**Table1**. Kinetic mechanism of heterogeneous catalytic olefin polymerization

| Description | Reaction | Kinetic constant |
|---|---|---|
| Activation | $C^k \rightarrow C^{*k}$ | $K_a^k$ |
| Initiation | $C^{*k} + M \rightarrow P_1^k$ | $K_i^k$ |
| Propagation | $P_n^k + M \rightarrow P_{n+1}^k$ | $K_p^k$ |
| Transfer | $P_n^k \rightarrow C^{*k} + D_n^k$ | $K_{tr}^k$ |
| Deactivation | $P_n^k \rightarrow C_d^k + D_n^k$<br>$C^{*k} \rightarrow C_d^k$ | $K_{dac}^k$ |

**Table 2**. Net production-consumption rates of the leading moments of "live" and "dead" polymer chain distributions

| |
|---|
| Fresh site<br>$R^e_{[C^k]^e} = -K_d^k [C^k]^e$ |
| Active site<br>$R^e_{[C^{*k}]^e} = -(K_{dac}^k + K_i^k [M]^e)[C^{*k}]^e + K_{tr}^k [\lambda_0^k]^e$ |
| 0-Moment of "live" chains<br>$R^e_{[\lambda_0^k]^e} = K_t^k [C^{*k}]^e [M]^e - (K_{tr}^k + K_{dac}^k)[\lambda_0^k]^e$ |
| 1-Moment of "live" chains<br>$R^e_{[\lambda_1^k]^e} = K_i^k [C^{*k}]^e [M]^e - (K_{tr}^k + K_{dac}^k)[\lambda_1^k]^e + K_p^k [\lambda_1^k]^e [M]^e$ |
| 2-Moment of "live" chains<br>$R^e_{[\lambda_2^k]^e} = K_i^k [C^{*k}]^e [M]^e - (K_{tr}^k + K_{dac}^k)[\lambda_2^k]^e + K_p^k ([\lambda_0^k]^e + 2[\lambda_1^k]^e)[M]^e$ |
| 0-Moment of "dead" chains<br>$R^e_{[\mu_2^k]^e} = (K_{tr}^k + K_{dac}^k)[\lambda_2^k]^e$ |
| 1-Moment of "dead" chains<br>$R^e_{[\mu_1^k]^e} = (K_{tr}^k + K_{dac}^k)[\lambda_1^k]^e$ |
| 2-Moment of "dead" chains<br>$R^e_{[\mu_2^k]^e} = (K_{tr}^k + K_{dac}^k)[\lambda_2^k]^e$ |

*Development of a two-dimensional particle growth model*

In the present study, in order to calculate the monomer concentration in a growing polymer particle a two-dimensional (in r and θ spherical coordinates) dynamic diffusion-reaction model was considered as depicted in Figure 1. Note that in the polymeric flow model (PFM) the polymer phase and the catalyst fragments are approximated by a pseudo-homogeneous medium. Under the above simplifying assumptions, the governing 2-D diffusion-reaction equation for the monomer concentration, M, in a growing catalyst/polymer particle can be written as follows:

**Table 3**. Numerical values of the kinetic rate constants [11-13]

| Dimension | Pre-exponential factor | | Description | Reaction constant |
|---|---|---|---|---|
| | Site 2 | Site 1 | | |
| 1/s | $6.12*10^5$ | $1.53*10^5$ | Activation | $K_a^k$ |
| $m^3$/s.mol | $6.12*10^6$ | $1.53*10^6$ | Initiation | $K_i^k$ |
| $m^3$/s.mol | $6.12*10^6$ | $1.53*10^6$ | Propagation | $K_p^k$ |
| 1/s | $3.83*10^6$ | $3.83*10^6$ | Transfer | $K_{tr}^k$ |
| 1/s | $2.5*10^2$ | $2.5*10^2$ | Deactivation | $K_{dac}^k$ |

All activation energies are assumed as 41.8 kJ/mol

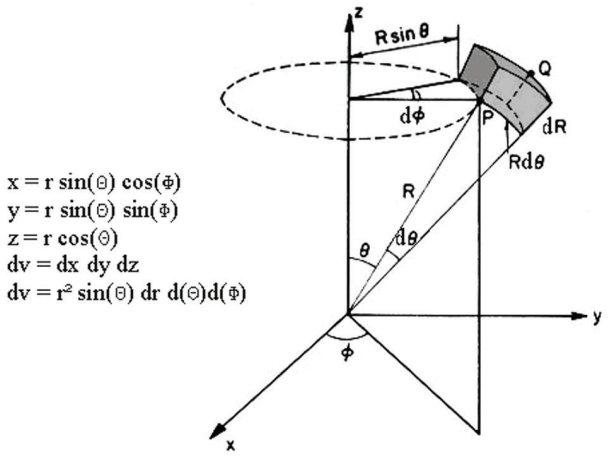


**Figure 1**. Spherical coordinates and their relations with Cartesian coordinates

$$\frac{\partial M}{\partial t}=\frac{1}{r^2}\frac{\partial}{\partial r}\left(Dr^2\frac{\partial M}{\partial r}\right)+\frac{1}{r^2\sin\theta}\frac{\partial}{\partial\theta}\left(D\sin\theta\frac{\partial M}{\partial\theta}\right)-R_P \quad ; \quad (r,\theta)\in\Omega_t \tag{4}$$

Boundary conditions:

$$M(r,\theta,t)=Ms \quad ; \quad (r,\theta)\in\{\Gamma_t - Z_{axis}\} \tag{5}$$

In symmetrical geometries, in which the symmetry line is the z axis, it is possible to use the symmetric conditions as a one-dimensional solution:

$$\frac{\partial M}{\partial\theta}=0 \quad ; \quad (r,\theta)\in\{\Gamma_t\cap Z_{axis}\} \tag{6}$$

Initial condition:

$$M(r,\theta,0)=0 \quad ; \quad (r,\theta)\in\Omega_0 \tag{7}$$

Where D is the monomer diffusion coefficient. Rp (mol/m$^3$.s) is the polymerization rate (Eq. 2). $\Omega_t$ and $\Gamma_t$ denote the internal and boundary particle domains at time t, respectively. $\Omega_0$ is the particle domain at time 0 and $M_s$ is the monomer concentration at the external particle surface.

Assuming that the all other molecular species in the growing polymer particle are not diffusion limited, the following dynamic 2-D conservation equation can be derived to describe the temporal-spatial distribution of the molar species (X: $C^k$, $C^{*k}$, $\mu_\nu^k$ and $\lambda_\nu^k$, $\nu$ =0,1 and 2 and k =1 and 2) in the growing particle.

$$\frac{\partial X}{\partial t}=\frac{1}{r^2}\frac{\partial}{\partial r}\left(r^2uX\right)+\frac{1}{r\sin\theta}\frac{\partial}{\partial\theta}\left(uX\sin\theta\right)+R_X \tag{8}$$

Boundary condition:

$$\int_{\Omega_t}\frac{dX}{dt}d\Omega_t=\oint_{\Gamma_t}Xud\Gamma_t \tag{9}$$

Initial condition:

$$X=(r,\theta,0)=X_0 \quad ; \quad (r,\theta)\in\Omega_0 \tag{10}$$

where $R_X$ is the net production/consumption rate of species X (Table 2). At time zero, the concentrations of $C_0^{*k}$, $\lambda_{\nu,0}^k$ and $\mu_{\nu,0}^k$ are equal to zero while the concentration of the catalyst fresh sites at time t=0, $C_0^k$, would be equal to a selected value (Table 4).

Due to polymer formation, the initial catalyst particle volume grows with time. Assuming that the polymer phase behaves as an incompressible medium, the following pseudo-steady state two-dimensional mass conservation equation is derived to describe the particle volume change with time:

$$\frac{1}{r^2}\frac{\partial}{\partial r}\left(r^2u\right)+\frac{1}{r\sin\theta}\frac{\partial}{\partial\theta}\left(u\sin\theta\right)-\frac{R_pM_{MW}}{\rho}=0 \ , \ (r,\theta)\in\Omega_t \tag{11}$$

**Table 4.** Physical, transport properties and catalyst characteristics [11-13]

| Dimension | Value | Description | |
|---|---|---|---|
| m²/s | $10^{-10}$ or $10^{-9}$ | Effective diffusion coefficient | D |
| mol/m³ | 2000 | Bulk concentration of monomer | $[M_s]$ |
| kg/m³ | 2840 | Catalyst density | $\rho_c$ |
| kg/m³ | 905 | Polymer density | $\rho_p$ |
| mol/kg$_{cat}$ | 5*10$^{-2}$ | Initial concentration of catalyst active sites of type 1 | $C_0^1$ |
| mol/kg$_{cat}$ | 5*10$^{-2}$ | Initial concentration of catalyst active sites of type 2 | $C_0^2$ |
| kgmol | 42*10$^{-3}$ | Molecular weight of monomer | $M_{mw}$ |
| m | 15*10$^{-6}$ | Initial catalyst radius | $R_0$ |
| kJ.mol | 100 | Heat of reaction | $\Delta H$ |
| kJ/kg.K | 2 | Heat capacity | $C_p$ |
| kJ/m²s | 1.5 | Heat transfer coefficient | H |
| K | 343 | Bulk temperature | $T_b$ |

Boundary condition:

$$\int_{\Omega_t} \frac{R_p M_{MW}}{\rho} d\Omega_t = \oint_{\Gamma_t} u d\Gamma_t \qquad (12)$$

where u (in $m^3/s.m^2$) denotes the flux volumetric flow rate of the growing polymer phase.

To study the overheating, lumped energy balance is used:

$$\int_{\Omega_t} R_p \Delta H d\Omega_t = h A_t (T_p - T_b) + m_t C_p \frac{dT_p}{dt} \qquad (13)$$

Initial condition:

$$T_p = T_b \quad ; \quad t = 0 \qquad (14)$$

where $T_p$ and $T_b$ are the particle and bulk phase temperatures, *h* is the external film heat transfer coefficient and $T_p$ and $T_b$ are the surface area and mass of particle at time t, respectively. Heat transfer between the bulk phase in the reactor and the particle surface is controlled by the film-side convective heat transfer coefficient "h". The value of the coefficient depends on the particle radius, fluid properties, and the relative particle/bulk phase velocities.

In the published literature, various correlations have been proposed to calculate the heat transfer coefficients for spherical particles in a flowing gas medium. In this regard several investigators have employed the Ranz-Marshall correlations for calculating the heat transfer coefficients for growing polymer particles in gas phase catalytic olefin polymerization [12, 14, 36-38]. It has been found that the Ranz-Marshall correlations often provide good predictions for heat or mass transfer coefficients for large particles, but it is not suitable for this system, especially for small and highly active catalyst particles; if assumed that the particle temperature is influenced by the transfer at the surface, then a heat transfer coefficient with two to three times higher than that predicted with the Ranz-Marshall correlation would be needed to maintain a particle temperature under the melting point of polymer [9, 16]. However, in this work based on the values reported by Floyd et al. [12], constant value for particle heat transfer coefficient, h, is applied. Different values for h inside cracks as a percent of particle heat transfer coefficient, is applied to show the significance of the ratio of two heat transfer coefficients on the particle temperature instead of a precise value particularly for inside the cracks.

If the fragments pattern makes any extra surface the revised form of Eq. (13) with extra term representing the heat transfer from extra surface created by radial cracks can be applied:

$$\int_{\Omega_t} R_p \Delta H d\Omega_t = h A_t (T_p - T_b) + h_c A_c (T_p - T_b) + m_t C_p \frac{dT_p}{dt} \qquad (15)$$

where $h_c$ and $A_c$ are transfer coefficients from extra surface and the extra surface area, respectively. Due to symmetry in φ direction of developed 2-D model, the indicator line of crack was rotated along Z axe to calculate the extra surface (Figure 3).

*Numerical approach to solve the governing equations*

The molecular and mass conservation equations, Eqs. (4-12), are numerically solved using a Galerkin finite element method combined with a finite

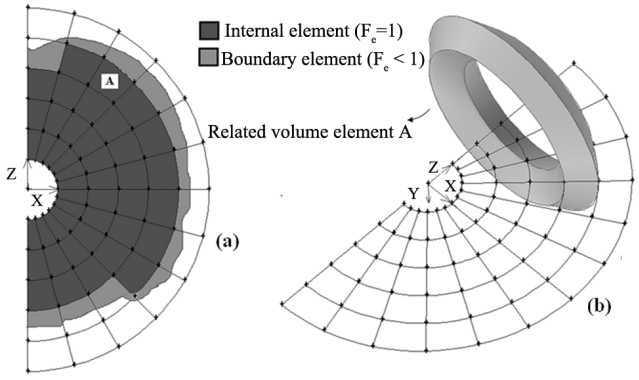


**Figure 2**. Particle domain and its discretization into 2-D finite elements (a) and 3-D volume elements obtained via the integration of the respective 2-D elements (b)

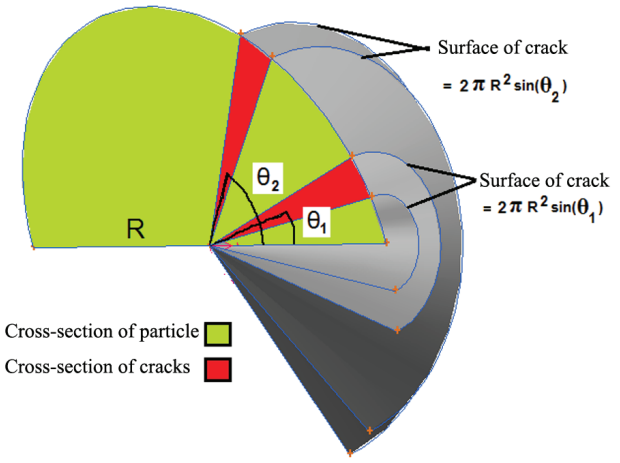


**Figure 3**. Schematic representation of calculating the cracks surface

differences technique. Accordingly, the computational domain is divided into a number of 2-D finite elements in the r and θ coordinates (Figure 2a). The initial catalyst particle was positioned in the center of the computational domain. To solve the resulting moving boundary value problem and follow the particle growth with time, a parameter known as fill factor was defined for each element, $F_e$. In particular, for an internal element (filled), the value of the fill factor was set equal to one ($F_e$ =1). For a boundary element (semi-filled), the value of $F_e$ varies from 0 to 1 while for all other elements outside the time-varying particle domain, the value of $F_e$ is equal to zero. As the particle grows the value of the fill factor for a boundary element changes from zero to 1 (i.e., a boundary element becomes an internal one). It should be noted that in Ziegler-Natta olefin polymerization, the catalyst particle diameter can increase up to 50 times of its initial size. Thus, to reduce the computational effort the total number of elements in the computational domain, $N_e$, progressively increases. In this regard the number of the selected discrete points in the θ direction is either 90 (i.e., =180°/90°=2°) or 180 (i.e., Δθ = 1°) but, the total number of discrete points in the r direction, $N_r$, varies with particle growth. Note that the concentrations of all the molecular species in each computational element changes with time and this may cause an essential challenge in computational time.

It should be noted that the monomer conservation Eq. (4) is solved in the 2-D computational domain using a Galerkin finite element numerical method. On the other hand, the molar species conservation Eq. (8) and the total mass conservation Eq. (11) are solved in the discrete volume elements obtained via the integration/rotation of the 2-D finite element domain with respect to the φ coordinate (i.e., from 0° to 360°, Figure 2b).

Due to the coupling of the monomer conservation equation in Eq. (4) with the molar species conservation rate equations, as in Eq. (8), and the total mass conservation equation of Eq. (11), an iterative numerical approach after their decoupling was employed to solve the resulting extremely large system of simultaneous ODEs and algebraic equations (e.g., over $16*N_e$). Figure 4 shows the flowchart of algorithm which is used to solve the equations. More details for solving Eqs. (4)-(12) are presented in Najafi et al.[33].

After calculating the values of all fluxes, the values of molar species concentration and the fill factors for each boundary elements are calculated by using the following equations:

$$V^e \frac{\partial (XF^e)}{\partial t} = \oint_{\Gamma^e} Xu^e .\, d\Gamma^e + V^e F^e R_X \tag{16}$$

$$\oint_{\Gamma^e} u.d\Gamma + F^e \frac{R_p M_{MW}}{\rho_p} = V^e \frac{\partial F^e}{\partial t} \tag{17}$$

Subsequently Eq. (13) is used to calculate particle temperature at each time step. At the end of each time step, the total number and weight average chain lengths in the particle ($\overline{X}_n$ and $\overline{X}_w$) are calculated using the following equations:

$$\overline{X}_n = \frac{\sum_{e=1}^{N_e} W_e}{\sum_{e=1}^{N_e} \frac{W_e}{\overline{X}_n^e}} \quad ; \quad \overline{X}_w = \frac{\sum_{e=1}^{N_e} W_e \overline{X}_w^e}{\sum_{e=1}^{N_e} W_e} \tag{18}$$

where $N_e$ is the number of finite elements, $W_e$, $\overline{X}_n^e$ and $\overline{X}_w^e$ are the polymer mass, number and weight average chain lengths of the polymer formed in the finite volume element "e".

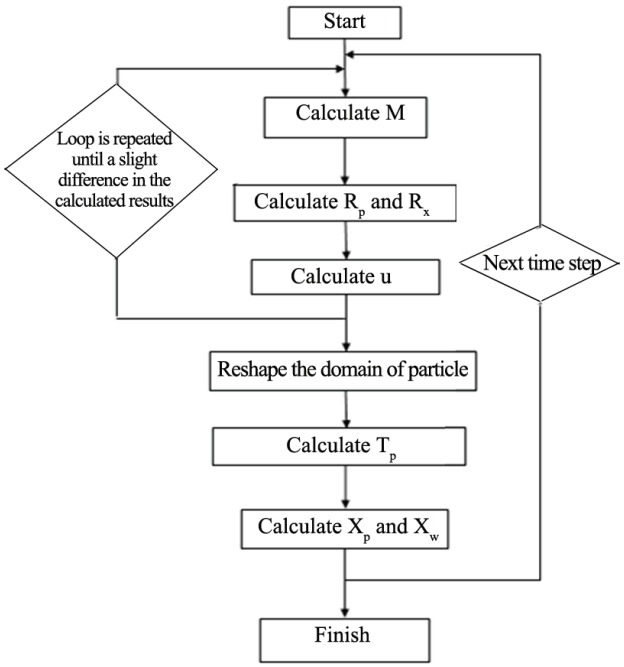


**Figure 4**. Computer code flowchart used to solve equations

## RESULTS AND DISCUSSION

The developed 2-D particle growth model is used to assess the effects of pores distribution patterns inside the particle on the spatial-temporal monomer distribution, polymerization rate profile, molecular weight average properties (i.e., $\overline{X}_n$, $\overline{X}_w$, PDI) and particle overheating of a single polymer particle in Z-N olefin polymerization.

In Tables 3 and 4, the numerical values of the kinetic rate constants and the values of various physical and transport properties and the selected polymerization conditions are reported.

In this work, to demonstrate the fragments inside the particle, using PFM assumption, two different diffusion coefficients were employed. The wide range for diffusion coefficient was represented in literature. In Floyd et al [11-13] the diffusion coefficient varied between $10^{-11}$ to $10^{-7}$ $m^2/s$ for gas phase and slurry polymerization. We used diffusion coefficient of $10^{-10}$ $m^2/s$ for elements located in filled part of the particle and $10^{-9}$ $m^2/s$ for elements located in pores (non-filled) zones of the particle.

To include the effect of fragment patterns inside the particle four different patterns were selected: radial pores, random pores, shell pores and combined pores. For each case two different sizes were selected while

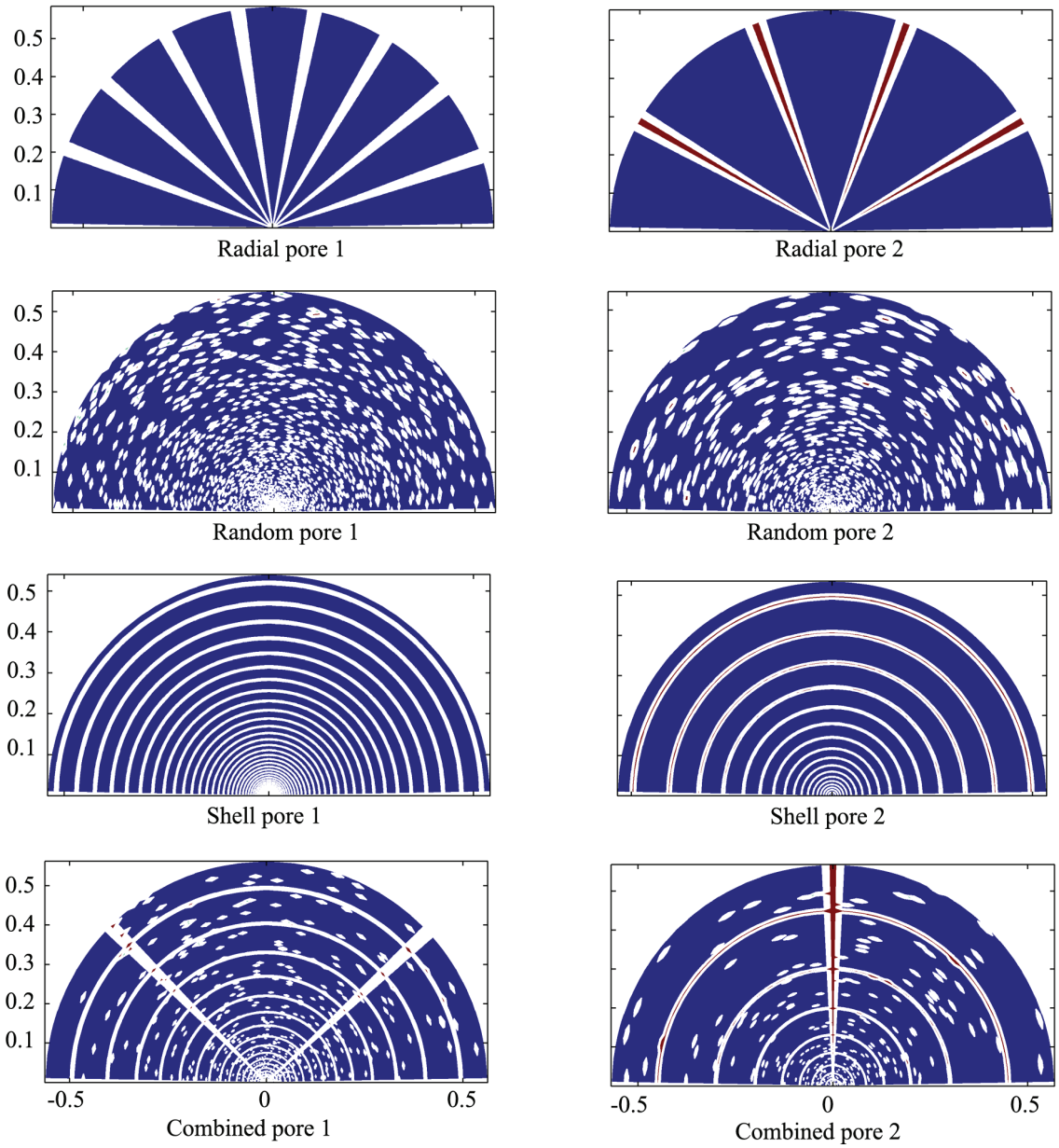


**Figure 5**. Fragment patterns: white zones indicate pores and blue zones indicate fragments (color version is available in issue No 2, Vol.1, in POJ Website)

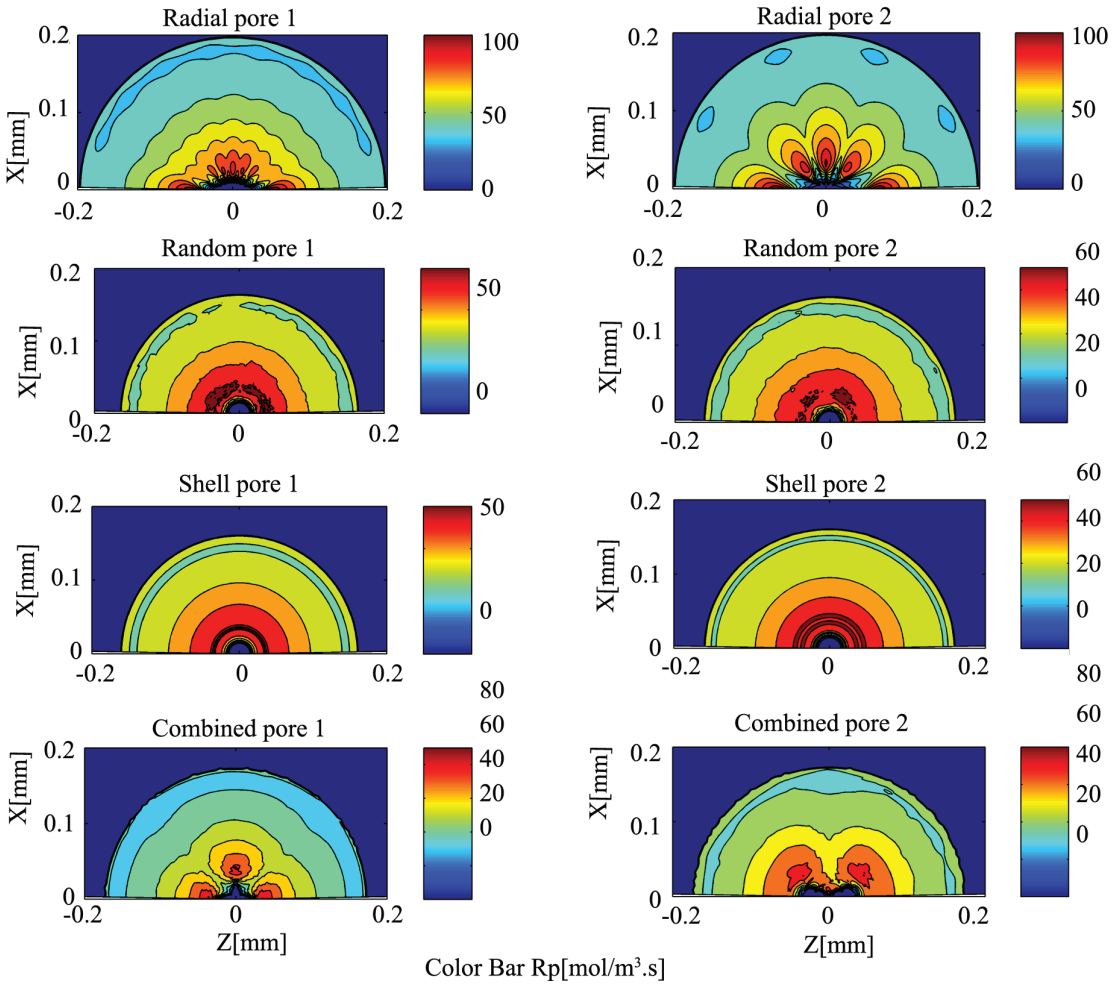


**Figure 6**. Local polymerization rate contours inside the particle for different cases after 600 s of polymerization (The colored version of this figure is available in issue No. 2, Vol. 1 of POJ website).

the total volume fraction of pores inside the particle for all cases was similar.

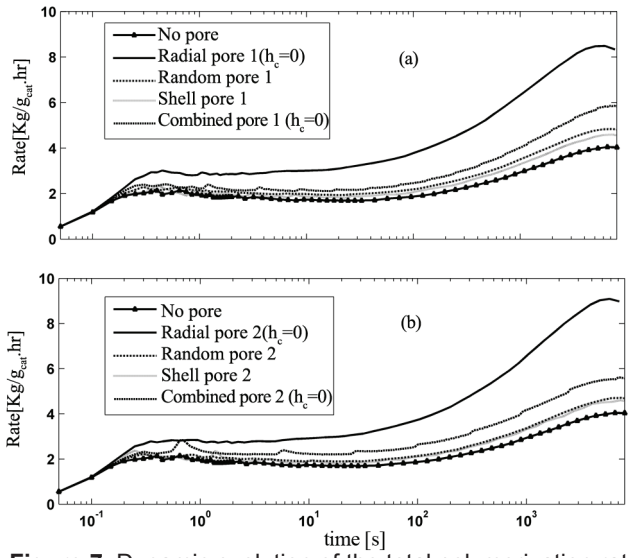


**Figure 7**. Dynamic evolution of the total polymerization rate for different patterns: (a) more and smaller pores (b) less and bigger pores

Figure 5 shows the selected patterns. The radial pore represents radial crack inside particle. In the cracks the diffusion coefficient is higher than inside fragments. It is $10^{-10}$ m$^2$/s for fragments and $10^{-9}$ m$^2$/s in cracks as stated in Table 4. The shell pore represents a shell fragmentation process and just ringed cracks are considered. For radial and combined pores pattern Eq. (15) is used to calculate the particle temperature while for two other cases (i.e., random pore and shell pore) Eq. (13) is used.

Figure 6 shows local polymerization rate contours inside the particle for different cases after 600 s. Since local polymerization rate is related to monomer and live chains concentrations, it can be concluded that the pattern considerably affects the concentrations inside the particle during the polymerization.

Figure 7 shows polymerization rate (productivity) versus time for different cases. As can be seen, all cases show higher polymerization rate in comparison with particles without any crack. Cases with radial

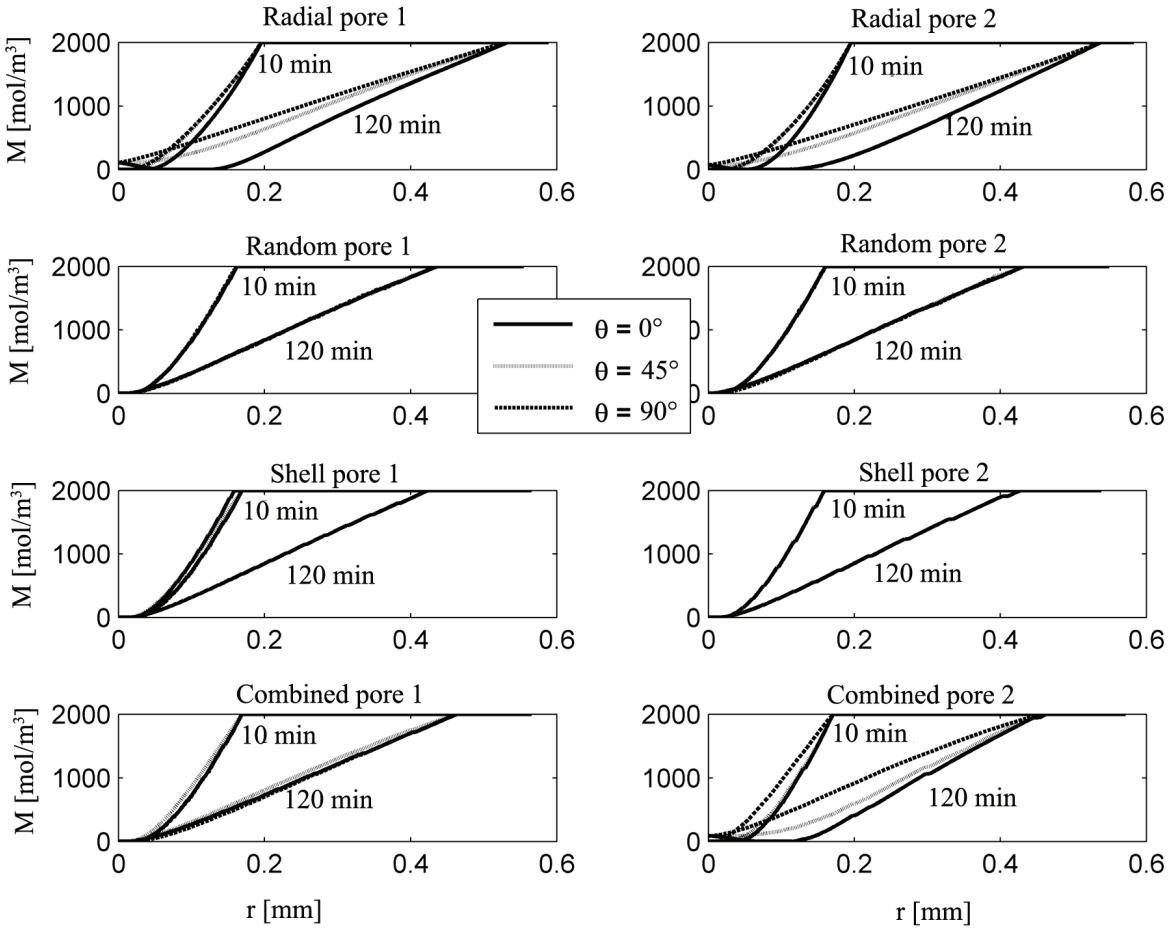


**Figure 8**. Monomer concentration at three different cross sections (θ = 0° , 45° and 90°) at 10 min and 120 min of the beginning of polymerization reaction for different patterns

pores show significantly more productivity because in these situations accessibility of monomer to catalyst sites inside the particle, especially at the center of particle is greater. It has to be noted that since the total volume fraction of pores inside the particle for all cases is similar, in the combined case the volume

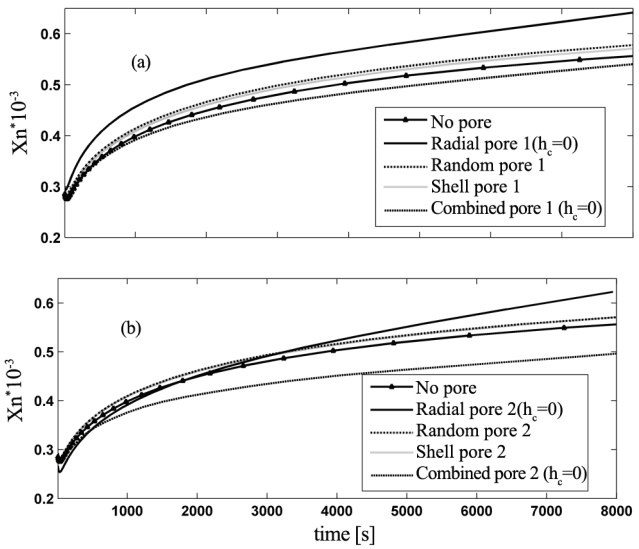


**Figure 9**. Dynamic evolution of the $\overline{X}_n$ for different patterns: (a) more and smaller pores and (b) less and bigger pores

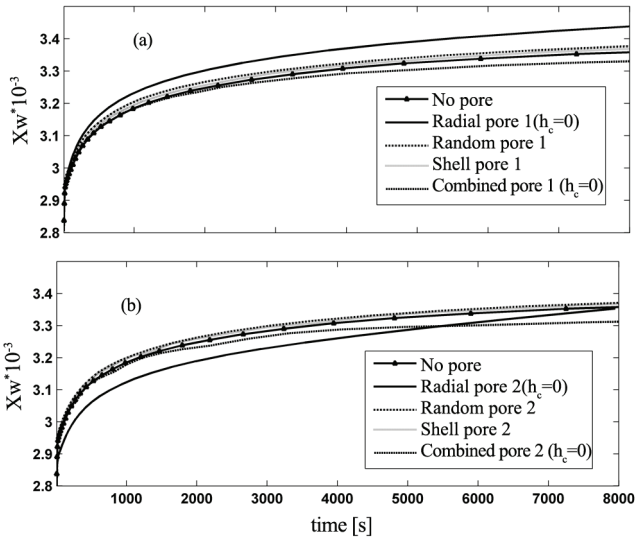


**Figure 10**. Dynamic evolution of the $\overline{X}_w$ for different patterns: (a) more and smaller pores and (b) less and bigger pores

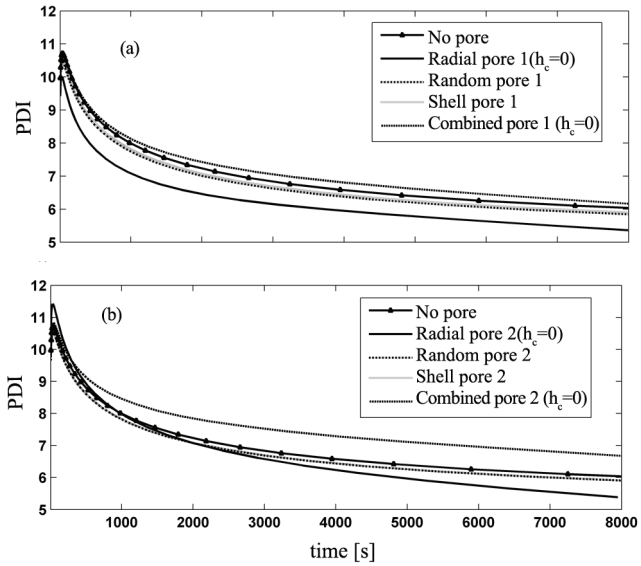


**Figure 11**. Dynamic evolution of the PDI for different patterns: (a) more and smaller pores and (b) less and bigger pores

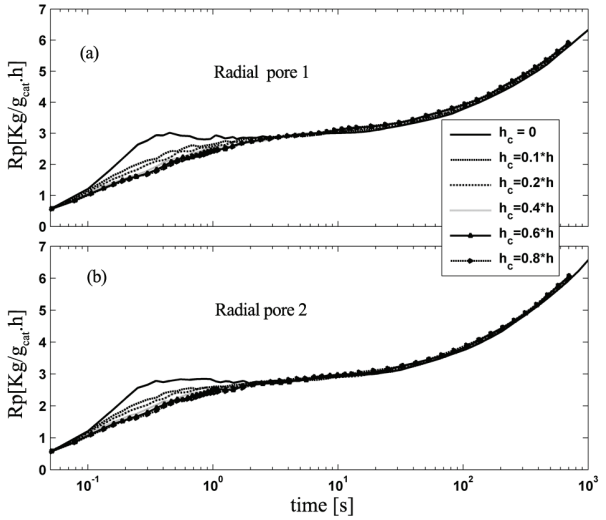


**Figure 13**. Dynamic evolution of the total polymerization rate of "radial pore" pattern for different value of $h_c$: (a) more and smaller pores and (b) less and bigger pores

of radial cracks is decreased in comparison with the case of just radial cracks and so the rate is lower than the radial cracks.

Monomer concentrations are shown in three different cross sections (i.e., $\theta = 0°$ , 45° and 90°) at 10 min and 120 min in Figure 8. The concentration curves at different cross sections coincide but not in cases of radial and combined pores. The concentration gradient for radial pore cases is decreased considerably while the concentration at the same positions are generally higher.

Number and weight average chain lengths of the polymer for different cases are shown in Figures 9 and 10. These Figures indicate that number average chain length has been affected by fragment patterns more than weight average chain length. Since, the number of radial cracks in the combined case is less than the radial case the number average chain length for the combined case is less than that of radial case. The number average chain length is more affected by the fragments pattern than the weight average chain length. Polydispersity index, PDI, for different cases are shown in Figure 11. As it can be seen the fragmentation pattern affects PDI. For example in the

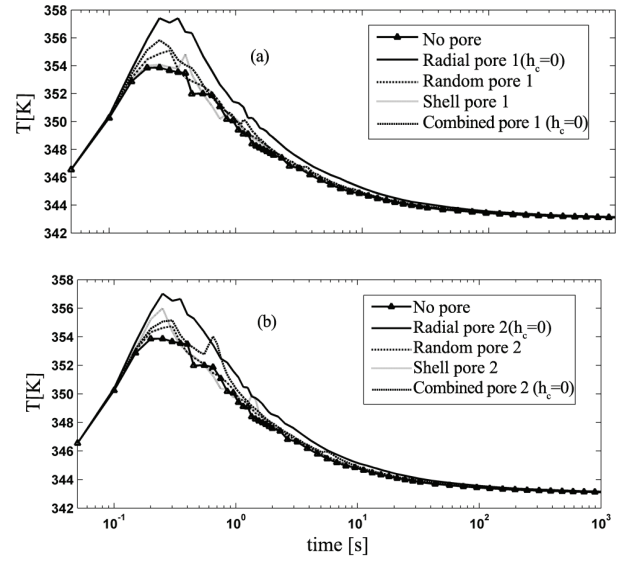


**Figure 12**. Dynamic evolution of the of particle temperature for different patterns: (a) more and smaller pores (b) less and bigger pores

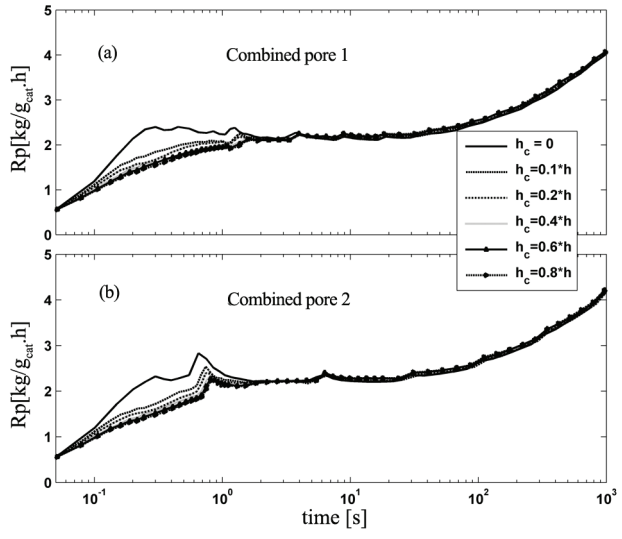


**Figure 14**. Dynamic evolution of the total polymerization rate of "combined pore" pattern for different value of $h_c$: (a) more and smaller pores (b) less and bigger pores

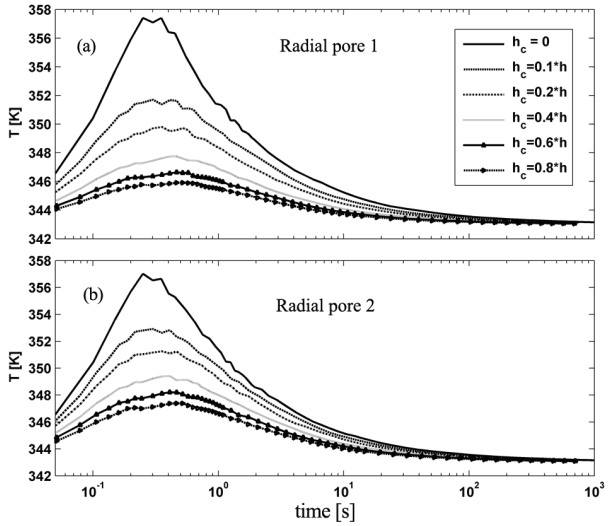


**Figure 15**. Dynamic evolution of particle temperature of "radial pore" pattern for different values of $h_c$: (a) more and smaller pores (b) less and bigger pores

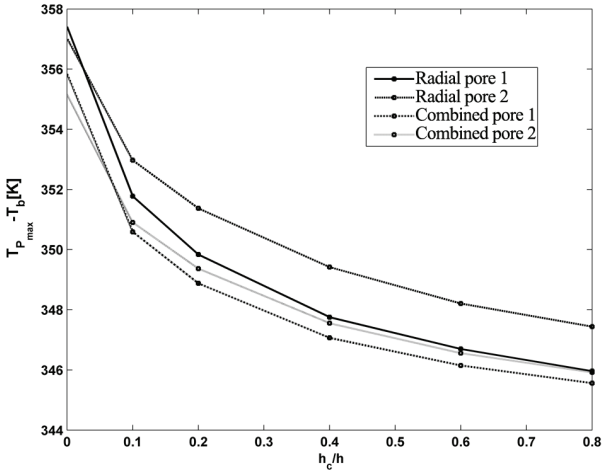


**Figure 17**. Maximum particle overheating for different values of $h_c$

combined case the PDI is considerably increased in comparison with other patterns.

Particle temperature versus time for all cases is shown in Figure 12. Since olefin polymerization reactions are highly exothermic, particle overheating is a challenging issue in these processes. This subject is more important at early stages of polymerization due to more concentration of active sites and low particle surface. Heat released by the reaction is high and heat transfer by the convection is low. Note that particle overheating can lead to higher probability of particles agglomeration. The modeling results show that particle and bulk temperature difference can be 10 to 15 degrees for different cases at first few seconds of reaction according to the selected values for heat transfer and diffusion coefficients. The maximum temperature appears for the radial pore distribution patterns because of higher polymerization rate when the heat transfer from radial cracks is neglected ($h_c$ = 0, in Figure 7).

To include heat transfer from radial cracks, the heat transfer coefficient from radial pores is considered to be a percent of external film heat transfer coefficient h. Figures 13 to 16 show the results of polymerization rate and particle overheating for radial and combined pore patterns with different selected values of $h_c$. As the Figures 15 and 16 show at early stages of polymerization the inclusion of heat transfer

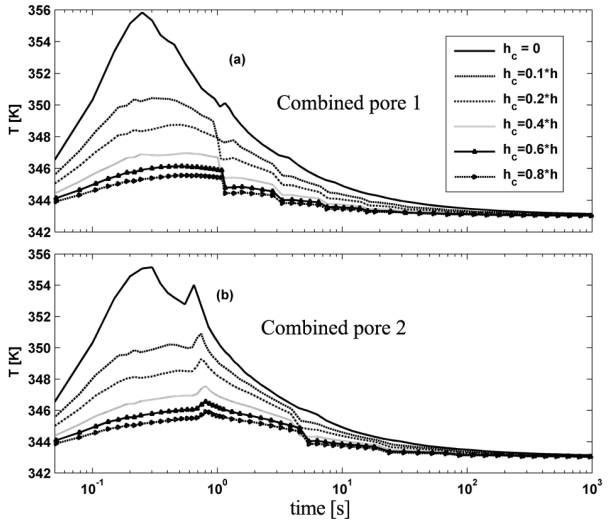


**Figure 16**. Dynamic evolution of particle temperature of "radial pore" pattern for different values of $h_c$: (a) more and smaller pores (b) less and bigger pores

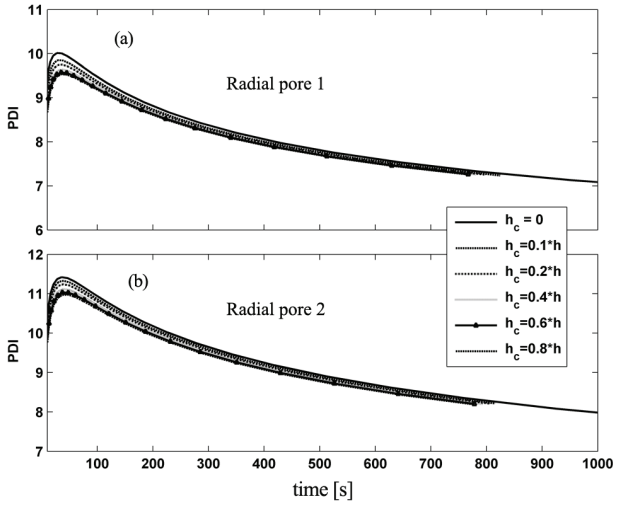


**Figure 18**. Dynamic evolution of PDI for particle with "radial pore" pattern and different values of $h_c$: (a) more and smaller pores and (b) less and bigger pores

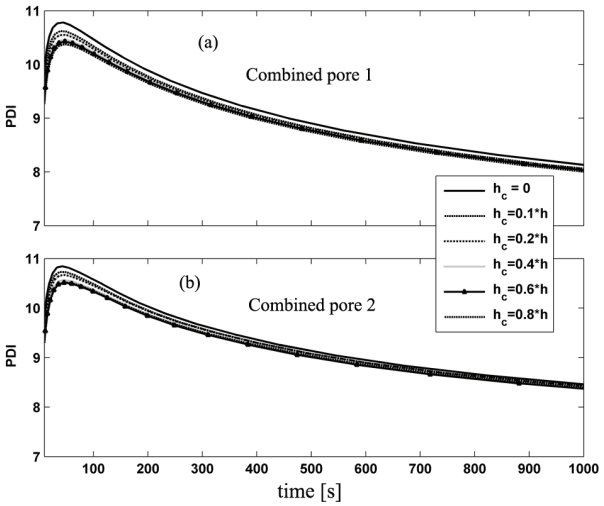


**Figure 19**. Dynamic evolution of PDI for particle with "combined pore" pattern and different values of $h_c$: (a) more and smaller pores (b) less and bigger pores

coefficient inside the particle reduces the reaction rate as the particle temperature is reduced. In combined cases as particle grows the new shell pores appear in the particle which increase the reaction rate and so a small jump in the rate can be seen. For combined cases as Figure 16 shows by appearance of new shell pores we have an increase in reaction rate and heat transfer rate which have opposite effects on particle temperature. At the early stages of polymerization in which the reaction rate is higher we have sudden increase in particle temperature and then we see a sudden reduction in particle temperature. As Figure 17 shows even with a low $h_c$ of about 0.1*h the particle temperature decreases dramatically. The reduction in overheating at early stages of polymerization plays significant role in decreasing the possibility of particle agglomeration. On the other hand as Figures 18 and 19 show changing the heat transfer coefficient inside the crack, $h_c$, has no considerable effect on the molecular properties of the final polymer.

## CONCULSION

A two-dimensional PFM model is used to simulate a single particle Ziegler-Natta olefin polymerization. A constant fragment pattern is applied to study the effect of cracks inside the particle on the molecular properties and particle temperature. Inclusion of cracks generally increases the monomer diffusion coefficient inside the particle. The results show that inclusion of cracks affects the molecular properties and reaction rate. Particularly the radial pore pattern increases the reaction rate and decreases the polydispersity index. The fragment patterns affect the particle temperature at early stages of polymerization considerably. Particularly the radial cracks by improving the heat transfer rate decrease the particle overheating. It has to be noted that the results are restricted to the patterns and the values and ratios of heat transfer and diffusion coefficients studied in this work. It is also important to note that each pattern imposes a fragment size and shape which are effective on reaction rate and molecular properties as studied by Najafi et al. [33].

## REFERENCES

1. McKenna TF, Soares JBP (2001) Single particle modelling for olefin polymerization on supported catalysts: A review and proposals for future developments. Chem Eng Sci 56: 3931–3949
2. McKenna TF, Di Martino A, Weickert G, Soares JBP (2010) Particle growth during the polymerisation of olefins on supported catalysts, 1-nascent polymer structures. Macromol React Eng 4: 40–64
3. Schmeal WR, Street JR (1971) Polymerization in expanding catalyst particles, AIChE J 17: 1188-1197
4. Singh D, Merrill RP (1971) Molecular weight distribution of polyethylene produced by Ziegler-Natta catalysts. Macromolecules 4: 599-604
5. Galvan R, Tirrell M (1986) Molecular weight distribution predictions for heterogeneous Ziegler-Natta polymerization using a two-site model. Chem Eng Sci 41: 2385-2393
6. Byrne GD (1993) The taming of co-polymerization problem with VODE. Impact Comput Sci Eng 5: 318-344
7. Hoel EL, Cozewith C, Byrne GD (1994) Effect of diffusion on heterogeneous ethylene propylene copolymerization. AIChE J 40: 1669-1684
8. Veera UP, Weickert G, Agarwal US (2002) Modeling monomer transport by convection during olefin polymerization. AIChE J 48: 1062-1070
9. Kanellopoulos V, Dompazis G, Gustafsson B, Kiparissides C (2004) Comprehensive analysis of single-particle growth in heterogeneous olefin

polymerization: The random - pore polymeric flow model. Ind Eng Chem Res 43: 5166-5180
10. Nagel EJ, Klrillov VA, Ray WH (1980) Prediction of molecular weight distributions for high-density polyolefins. Ind Eng Chem Prod Res Dev 79: 372-379
11. Floyd S, Choi KY, Taylor TW, Ray WH(1986) Polymerization of olefins through heterogeneous catalysis. III. Polymer particle modelling with an analysis of intra particle heat and mass transfer effects. J Appl Polym Sci 32: 2935-2960
12. Floyd S, Choi KY, Taylor TW, Ray WH (1986) Polymerization of olefins through heterogeneous catalysis. IV. Modeling of heat transfer resistance in the polymer particle boundary Layer. J Appl Polym Sci 31: 2231-2265
13. Floyd S, Heiskanen T, Taylor TW, Mann GE, Ray WH (1987) Polymerization of olefins through heterogeneous catalysis. VI. Effect of particle heat and mass transfer on polymerization behavior and polymer properties. J Appl Polym Sci 33: 1021-1065
14. Hutchinson RA, Chen CM, Ray WH (1992) Polymerization of olefins through heterogeneous catalysts X: Modelling of particle growth and morphology. J Appl Polym Sci 44: 1389
15. Weickert G, Meier GB, Pater JTM, Westerterp KR (1999) The particle as a microreactor: Catalytic propylene polymerization with supported metallocene and Ziegler–Natta catalysis. Chem Eng Sci 54: 3291
16. Mckenna TF, Dupuy J, Spitz R (1995) Modeling of transfer phenomena on heterogeneous Ziegler catalysts: Differences between theory and experiment in olefin polymerization (an introduction). J Appl Polym Sci 57: 371-384
17. Mckenna TF, Dupuy J, Spitz R (1997) Modeling of transfer phenomena on heterogeneous Ziegler catalysts. III. Modeling of intraparticle mass transfer resistance. J Appl Polym Sci 63: 315–322
18. Mckenna TF, Mattioli V (2001) Progress in describing particle growth for polyolefins: A look at particle morphology, Macromol Symp 173: 149-162
19. Kosek J, Grof Z, Novak A, Stepanek F, Marek M (2001) Dynamics of particle growth and overheating in gas-phase polymerization reactors. Chem Eng Sci 56: 3951–3977
20. Dompazis G, Kanellopoulos V, Touloupides V, Kiparissides C (2008) Development of a multi-scale, multi-phase, multi-zone dynamic model for the prediction of particle segregation in catalytic olefin polymerization FBRs. Chem Eng Sci 63: 4735-4753
21. Ferrero MA, Chiovetta MG (1987) Catalyst fragmentation during propylene polymerization: Part I: The effects of grain size and structure. Polym Eng Sci 27: 1436
22. Ferrero MA, Chiovetta MG (1987) Catalyst fragmentation during propylene polymerization: Part II: Microparticle diffusion and reaction effects. Polym Eng Sci 27: 1448-1460
23. Alexiadis A, Andes C, Ferrari D, Korber F, Hauschild K, Bochmann M, Fink G (2004) Mathematical modeling of homopolymerization on supported metallocene catalysts. Macromol Mater Eng 289: 457–466
24. Bonini F, Fraaije V, Fink G (1995) Propylene polymerization through supported metallocene/MAO catalysts: kinetic analysis and modelling. J Polym Sci Part A Polym Chem 33: 2393-2402
25. Kittilsen P, Svendsen H, Mc Kenna TF, Jakobsen HA, Fredriksen SB (2001) The interaction between mass transfer effects and morphology in heterogeneous olefin polymerization. Chem Eng Sci 56: 4015-4024
26. Kittilsen P, Svendsen H, Mc Kenna TF (2003) Viscoelastic model for particle fragmentation in olefin polymerization. AIChE J 49: 1495-1507
27. Kittilsen P, Svendsen H (2004) Three-level mass-transfer model for the heterogeneous polymerization of olefins. J Appl Polym Sci 91: 2158–2167
28. Grof Z, Kosek J, Marek M (2005) Modeling of morphogenesis of growing polyolefin particles. AIChEJ 51: 2048–2067
29. Grof Z, Kosek J, Marek, M (2005) Principles of the morphogenesis of polyolefin particles. Ind Eng Chem Res 44:2389-2404
30. Horackova B, Grof Z, Kosek J (2007) Dynamics of fragmentation of catalyst carriers in catalytic polymerization of olefins. Chem Eng Sci 62: 5264-5270
31. Bobak M, Gregor T, Bachman B, Kosek J (2008) Estimation of morphology characteristics of porous poly (propylene) particles from degassing measurements. Macromol React Eng 2: 176–189
32. Machado F, Lima EL, Pinto JC, Mc Kenna TF

(2001) An experimental study on the early stages of gas-phase olefin polymerizations using supported Ziegler–Natta and metallocene catalysts. Polym Eng Sci 51: http://onlinelibrary.wiley.com/doi/10.1002/pen.v51.2/issuetoc302–310

33. Najafi M, Parvazinia M, Ghoreishy MHR, Kiparissides C (2013) Development of a 2D single particle model to analyze the effect of initial particle shape and break agein olefin polymerization. Macromol React Eng 8: 29-45
34. Hatzantonis H, Yiannoulakis H, Yiagopoulos A, Kiparissides C (2000) Recent developments in modeling gas-phase catalyzed olefin polymerization fluidized-bed reactors: The effect of bubble size variation on the reactor's performance. Chem Eng Sci 55: 3237-3259
35. De Carvalho AB, Gloor PE, Hamielec AE (1989) A kinetic mathematical model for heterogeneous Ziegler-Natta copolymerization. Polymer 30: 280–296
36. Mc Auley KB, Mac Gregor JF, Hamielec AE (1990) Kinetic model for industrial gas-phase ethylene copolymerization. AIChE J 36: 837-850
37. Sun J, Eberstein C, Reichert KH (1997) Particle growth modeling of gas phase polymerization of butadiene. J Appl Polym Sci 64: 203-212
38. Yiagopoulos, A, Yiannoulakis H, Dimos V, Kiparissides C (2001) Heat and mass transfer phenomena during the early growth of a catalyst particle in gas-phase olefin polymerization: the effect of prepolymerization temperature and time. Chem Eng Sci 56: 3979–3995